Heliyon 10 (2024) e29504

Contents lists available at ScienceDirect

Heliyon

journal homepage: www.cell.com/heliyon

Research article

An integrated analysis revealing the angiogenic function of TP53I11 in tumor microenvironment

Wen Bai [a,b,1], Jun-Song Ren [a,b,1], Ke-ran Li [a,b,**], Qin Jiang [a,b,*]

[a] The Affiliated Eye Hospital, Nanjing Medical University, Nanjing, China
[b] The Fourth School of Clinical Medicine, Nanjing Medical University, Nanjing, China

ARTICLE INFO

Keywords:
TP53I11
Prognosis
Immune infiltration
Endothelial cells
Angiogenesis

ABSTRACT

Despite growing evidence suggesting an important contribution of Tumor Protein P53 Inducible Protein 11 (TP53I11) in cancer progression, the role of TP53I11 remains unclear. Our first pan-cancer analysis of TP53I11 showed some tumor tissues displayed reduced TP53I11 expression compared to normal tissues, while others exhibited high TP53I11 expression. Meanwhile, TP53I11 expression carries a particular pan-cancer risk, as high TP53I11 expression levels are detrimental to survival for BRCA, KIRP, MESO, and UVM, but to beneficial survival for KIRC. We demonstrated that TP53I11 expression negatively correlates with DNA methylation in most cancers, and the S14 residue of TP53I11 is phosphorylated in several cancer types. Additionally, TP53I11 was found to be associated with endothelial cells in pan-cancer, and functional enrichment analysis provided strong evidence for its role in tumor angiogenesis. In vitro angiogenesis assays confirmed that TP53I11 can promote angiogenic function of human umbilical vein endothelial cells (HUVECs) in vitro. Mechanistic investigations reveal that TP53I11 is transcriptionally up-regulated by HIF2A under hypoxia.

1. Introduction

The successful implementation of human genome projects in recent years has made people realize that a deeper understanding of human genetics is required because of the complexity of various forms of cancer [1,2]. A comprehensive cross-cancer examination of genes is crucial for determining their clinical prognostic value and identifying potential targets for cancer therapy. The value of pan-cancer analysis lies in its ability to uncover correlations between a particular gene and its clinical outcome, as well as its potential molecular mechanisms across a wide range of cancers [3,4]. Furthermore, this type of analysis enables the comprehensive examination of human cancers and helps identify similarities, disparities, and emerging trends [5,6].

The Tumor Protein P53 Inducible Protein 11 (TP53I11), also known as PIG11, is located on the human chromosome 11p11.2 [7]. In 1997, Polyak et al. first discovered that high p53 expression significantly induced multiple genes using Serial Analysis of Gene Expression technology when studying the mechanism of p53-dependent apoptosis in human colon cancer cells [8]. TP53I11 was one of the genes identified in the study. Studies have shown that TP53I11 is primarily expressed in the mammary gland, liver, and gastrointestinal tract, as well as in the corresponding cancer tissues [9]. Research has also linked TP53I11 to the development and

* Corresponding author. The Affiliated Eye Hospital, Nanjing Medical University, Nanjing, China.
** Corresponding author. The Affiliated Eye Hospital, Nanjing Medical University, Nanjing, China.
E-mail addresses: kathykeran860327@126.com (K.-r. Li), jqin710@vip.sina.com (Q. Jiang).
[1] These authors have contributed equally to this work.

https://doi.org/10.1016/j.heliyon.2024.e29504
Received 24 May 2023; Received in revised form 8 April 2024; Accepted 9 April 2024

progression of various types of tumors, including non-small cell lung, breast, liver, and gastric cancers. However, the role of TP53I11 in cancer remains a topic of ongoing research and debate in the scientific community. Some studies suggest that TP53I11, a downstream target gene of p53, may act as a tumor suppressor [10–13]. In vitro experiments have indicated the suppression of epithelial-mesenchymal transition and metastasis in breast cancer cells [12] and enhanced apoptosis in liver cancer cells [10,11]. Conversely, other studies have suggested that TP53I11 may play a role in promoting the development and progression of certain cancers [9,14]. In a recent bioinformatics study, it was found that breast cancer has a considerably elevated expression of TP53I11, and patients with low levels of expression tend to have a better survival rate [14]. High levels of TP53I11 have also been found to be prevalent in gastric cancer and have been shown to be strongly correlated with increased invasive depth, lymph node metastasis, distant metastasis, advanced staging [tumor (T), nodes (N), and metastases (M) (TNM)], and decreased overall survival in patients with gastric cancer [9]. Elevated levels of TP53I11 have also been linked to elevated serum levels of carcinoembryonic antigens [9]. Thus, further research is needed to clarify the role of TP53I11 in cellular processes and determine its potential as a therapeutic target for cancer treatment.

In summary, TP53I11 is a noteworthy gene that may significantly affect cancer biology and treatment. Further investigations are required to completely understand its involvement in the development and progression of diseases. In this study, we conducted a thorough assessment of TP53I11 with regard to transcription, clinical prognosis, DNA methylation, protein phosphorylation, immune infiltration, and functional enrichment in various cancer types, as well as an experimental validation in HUVECs.

2. Materials and methods

2.1. TP53I11 gene expression analysis

TP53I11 expression data in pan-cancer tissues and corresponding adjacent tissues were downloaded from the Human Protein Atlas (HPA) database (http://www.proteinatlas.org/) [15] and Gene Expression Profiling Interactive Analysis 2 (GEPIA2) database (http://gepia2.cancer-pku.cn/) [16]. The HPA database is publicly available and provides comprehensive information on the localization and expression of human proteins in different tissues and organs. The database was created with the goal of mapping the entire human proteome and contains information on over 20,000 proteins, including their tissue-specific expression patterns, antibody validation, and cellular localization. The GEPIA2 database provides a user-friendly interface that allows researchers to easily visualize and analyze gene expression data for various cancer types. This database contains over 20,000 samples from The Cancer Genome Atlas (TCGA) and

Table 1
Abbreviations and corresponding full names of various cancers.

Abbreviation	Full Name
ACC	Adrenocortical carcinoma
BLCA	Bladder urothelial carcinoma
BRCA	Breast invasive carcinoma
CESC	Cervical squamous cell carcinoma and endocervical adenocarcinoma
CHOL	Cholangio carcinoma
COAD	Colon adenocarcinoma
DLBC	Lymphoid neoplasm diffuse large B-cell lymphoma
ESCA	Oesophageal carcinoma
GBM	Glioblastoma multiforme
HNSC	Head and neck squamous cell carcinoma
KICH	Kidney chromophobe
KIRC	Kidney renal clear cell carcinoma
KIRP	Kidney renal papillary cell carcinoma
LAML	Acute myeloid leukaemia
LGG	Brain lower grade glioma
LIHC	Liver hepatocellular carcinoma
LUAD	Lung adenocarcinoma
LUSC	Lung squamous cell carcinoma
MESO	Mesothelioma
OV	Ovarian serous cystadenocarcinoma
PAAD	Pancreatic adenocarcinoma
PCPG	Pheochromocytoma and paraganglioma
PRAD	Prostate adenocarcinoma
READ	Rectum adenocarcinoma
SARC	Sarcoma
SKCM	Skin cutaneous melanoma
STAD	Stomach adenocarcinoma
TGCT	Testicular germ cell tumors
THCA	Thyroid carcinoma
THYM	Thymoma
UCEC	Uterine corpus endometrial carcinoma
UCS	Uterine carcinosarcoma
UVM	Uveal melanoma

the Chinese Cancer Genome Atlas (CGGA), making it one of the largest public transcriptome data resources; abbreviations and corresponding full names of various cancers are listed in Table 1.

2.2. Survival and prognosis analysis

Overall survival (OS), disease-free survival (DFS), and disease-specific survival (DSS) data were downloaded from the GEPIA2 and Gene Set Cancer Analysis (GSCA) databases (http://bioinfo.life.hust.edu.cn/GSCA/#/) [17]. In the context of survival curves, the GEPIA2 database was used to explore the relationship between gene expression patterns and patient outcomes, such as OS or DFS. The GSCA database was used to explore the relationship between gene methylation patterns and patient outcomes, such as OS, DFS, and DSS. In the context of the GEPIA2 or GSCA databases, the analysis of survival curves typically involves the use of statistical methods, such as Cox proportional hazards regression or Kaplan-Meier analysis. The results of the analyses were visualized using survival plots.

2.3. DNA methylation analysis

The DNA methylation levels were obtained from the GSCA database. The GSCA database provides a comprehensive collection of DNA methylation data from a wide range of samples, including tissues from different organisms and cell lines.

2.4. Protein phosphorylation analysis

Specific phosphorylation sites were identified using the UALCAN web portal (http://ualcan.path.uab.edu/). UALCAN is a web portal that provides a platform for exploring and analyzing proteomic data. The portal contains raw data from the Clinical Proteomic Tumor Analysis Consortium (CPTAC) dataset—a large repository of proteomic data on various types of cancer. These data include both total protein and phosphoprotein data, which can be used to study the phosphorylation status of proteins in cancer. These data are generated by the Clinical Proteomic Tumor Analysis Consortium (NCI/NIH). Upstream kinases were predicted via Kinase Enrichment Analysis (KEA) using the ARCHS4 database (available at https://maayanlab.cloud/archs4/) [18].

2.5. Single-cell sequencing data analysis

CancerSEA (http://biocc.hrbmu.edu.cn/CancerSEA/home.jsp) [12] is a specialized database for single-cell sequencing data related to cancer. It provides functional information at the single-cell level. We obtained correlation data for TP53I11 expression and various functional statuses of tumors from CancerSEA using single-cell sequencing data and generated a heatmap. Single-cell gene expression analysis in cancer tissues was performed using the IMMUcan SingleCell RNAseq database (https://immucanscdb.vital-it.ch/) [19]. IMMUcan can provide single-cell analysis of the tumor microenvironment (TME), which allows for the characterization of specific molecular profiles in individual cells rather than in bulk tissues. Single-cell gene expression analysis in normal tissues was performed using the EC Atlas database [20] (https://endotheliomics.shinyapps.io/ec_atlas/) and Murine ECTax database [21] (https://endotheliomics.shinyapps.io/murine_ectax/). The EC Atlas database contains the single cell transcriptome of murine ECs from 11 normal tissues (including brain, colon, extensor digitorum longus (EDL), heart, kidney, liver, lung, small intestine, soleus, spleen and testis) and Murine ECTax database contains the single cell transcriptome of murine ECs from choroid. The two-dim diagrams of all the individual ECs were obtained directly from the EC Atlas and Murine ECTax database. Single-cell gene expression analysis in lung tumors was analyzed with Seurat (v4.0) based on the Lung Tumor ECTax database [22](https://ccb.sites.vib.be/software-tools/lungTumor_ECTax).

2.6. Immune infiltration analysis

The TCGA data for the infiltration of 22 immune cells was obtained from the TIMER database (http://timer.cistrome.org/infiltration_estimation_for_tcga.csv.gz), which was then used to examine the relationship between TP53I11 expression and immune cell infiltration levels across different cancer types, as determined by XCELL algorithms. Additionally, the TIMER2 database (http://timer.cistrome.org/) [23], a comprehensive resource for analyzing immune cell infiltration, was used to confirm the correlation between TP53I11 expression and EC infiltration in different cancer types.

2.7. TP53I11-related functional enrichment analysis

Gene Ontology (GO) and Kyoto Encyclopedia of Genes and Genomes (KEGG) are two commonly used databases for the functional analysis of specific genes. GO provides information on the biological role of a gene set, whereas KEGG provides information on the molecular pathways and interactions in which a gene set is involved. The top 100 TP53I11-related genes were retrieved by utilizing the "Similar Gene Detection" module from the GEPIA2 database and subsequently inputted into the Enrichr web tool (https://maayanlab.cloud/Enrichr/) [24]for GO analysis. Gene Set Enrichment Analysis (GSEA) [25] is another computational approach that identifies biologically significant processes by evaluating a gene list that has been pre-ranked based on Log2FC values from a limma analysis [26]. The normalized enrichment score (NES) was calculated. A high NES score suggested that the gene set was significantly enriched among the top- or bottom-ranked genes, whereas a low NES score suggested that the gene set was not enriched. Gene functions were predicted using the ARCHS4 database, which is based on machine learning algorithms and provides a quick and reliable method for

estimating gene functions.

2.8. Cell culture and transfection

Human umbilical vein endothelial cells (HUVECs/TERT 2) were obtained from ATCC and were cultured in complete medium (i.e. EBM-2 medium plus EGM-2 Bullet Kit supplements, Lonza) containing 10 % fetal bovine serum (FBS). The cells were maintained in an environment containing 5 % CO2 at 37 °C to mimic the conditions found in the human body. In vitro angiogenesis assays, including fibrin bead angiogenesis assay, tube formation assay, 5-ethynyl-2′-deoxyuridine (EdU) assay and Transwell assay, were performed on HUVECs following a 24-h exposure to either hypoxic conditions (1 % O_2) or normoxic conditions (21 % O_2). All images were recorded using an inverted microscope (Olympus Corp, IX73P1F). For overexpression, overexpression plasmids pEX-4 (pGCMV/MCS/T2A/EGFP/Neo) for TP53I11(oeTP53I11), and mock control (vector) were obtained from GenePharma (Shanghai, China). For knocking down, siRNA against HIF-1α and HIF-2α were obtained from Genechem (Shanghai, China). The target sequence was as follows: siHIF-1α: 5′-GGGAUUAACUCAGUUUGAATT-3′, siHIF-2α: 5′- GGAGCUAACAGGACAUAGUTT-3′, siNC: 5′-GCGCGATAGCGCTAATAATTT-3’. For knocking out, CRISPR/Cas9-TP53I11–KO lentiviral constructs were obtained from Genechem (Shanghai, China). The sgRNA was as follows: koTP53I11 #1: 5′-ACCCGCAAGATCCTCGGCGT-3′, koTP53I11#2: 5′-ACCGCCGTAGAGGCGGATGG-3′, koNC: 5′-CGCTTCCGCGGCCCGTTCAA-3’. HUVECs were incubated with lentiviral particles for 24 h and selected with 2.5 mg/mL puromycin.

2.9. Fibrin bead angiogenesis assay

According to the manufacturer’s protocol, bead solution (Sigma-Aldrich, C3275-10G), fibrinogen (Sigma-Aldrich, F8630-1G), aprotinin (Sigma-Aldrich, A1153), and thrombin stock solutions (Sigma-Aldrich, T4648-1KU) were prepared separately. HUVECs were trypsinized and mixed with bead solution by inverting the tube every 20 min for 4 h and cultured overnight. On day 2, beads coated with HUVECs were transferred to a conical tube, washed and dispersed in a fibrinogen/aprotinin mixture, and added to a pre-coated 24-well plate with thrombin solution. We randomly captured six fields per sample on day 7 and calculated the average bead sprouting length per sample using the Sprout Morphology plugin in Fiji (ImageJ).

2.10. Tube formation assay

Briefly, 4×10^4 HUVECs were seeded into a 24-well plate per well that was pre-coated with BD Matrigel Matrix (Corning, 356234). Following an overnight incubation period, the tube-like structures were photographed. The tube formation length was analyzed using the Fiji (ImageJ) Angiogenesis Analyzer plugin.

2.11. EdU assay

According to the manufacturer’s instructions, HUVECs were incubated with EdU solutions at 20 μM for 4 h, and then stained using the EdU Assay kit (Biotime, C0071). The EDU positive cells (proliferating cells) were manually counted using the Fiji (ImageJ) software.

2.12. Transwell assay

Briefly, 4×10^4 HUVECs were placed in the top part of a specialized insert with small holes (8 μm PET, 24-well Millicell) containing serum-free medium. Meanwhile, the lower chambers were filled with 10 % FBS DMEM medium to encourage the cells to move through the holes. After 16 h, the cells on the bottom of the plate were fixed and stained in 0.05 % crystal violet solution (Sigma-Aldrich, 548-62-9) for 40 min. For photography, the cells on the top were removed by a cotton swab. The number of cells that migrated through the holes was manually counted using the Fiji (ImageJ) software.

2.13. Immunofluorescence

Immunofluorescent labeling of HUVECs was conducted using an anti-TP53I11 primary antibody (Abcam, ab234860, IF 1:50) followed by an Alexa 488-conjugated secondary antibody (Abcam, ab150077, IF 1:400). Subsequently, HUVECs were stained with rhodamine-conjugated phalloidin (Abcam, ab235138, 1:1000) and DAPI (Abcam, ab228549, 1:1000) to visualize the actin cytoskeleton and nuclei, respectively.

2.14. Western blot

Proteins from HUVECs were extracted using RIPA lysis buffer (Beyotime, P0013B) with a protease inhibitor mixture (Roche, 11697498001), and their concentration was determined using the Pierce BCA Protein Assay Kit (Thermo Fisher Scientific, 23225). The protein concentration was adjusted to 1 mg/ml using 5x SDS-PAGE sample loading buffer and then separated by SDS-PAGE in 1x running buffer (14.4g glycine, 2.9g tris base, and 1g SDS per 1 L distilled water). The separated proteins were transferred to a 0.45 μm PVDF membrane (Millipore, IPVH0010) using 1x transfer buffer (7.2g glycine, 1.45g tris base, and 20 % methanol per 1 L distilled water) and blocked with 5 % skim milk. The appropriate primary antibodies and secondary antibodies ere used to detect the target

protein bands, which were visualized using an Enhanced Chemiluminescence kit (Thermo Fisher Scientific, 32132). The following primary antibodies were used: rabbit anti-TP53I11 antibody (ABclonal, A12855, 1:500), mouse anti-HIF1A antibody (Novus, NB100-105,1:1000), rabbit anti-HIF2A antibody (Novus, NB100-122,1:1000). The mouse anti-β-actin (Millipore, A5441, 1:1000) was used as a protein loading control. The following secondary antibodies were used: goat anti-mouse HRP-conjugated antibodies (Beyotime, A0216; 1:1000) and goat anti-rabbit HRP-conjugated antibodies (Beyotime, A0208; 1:1000).

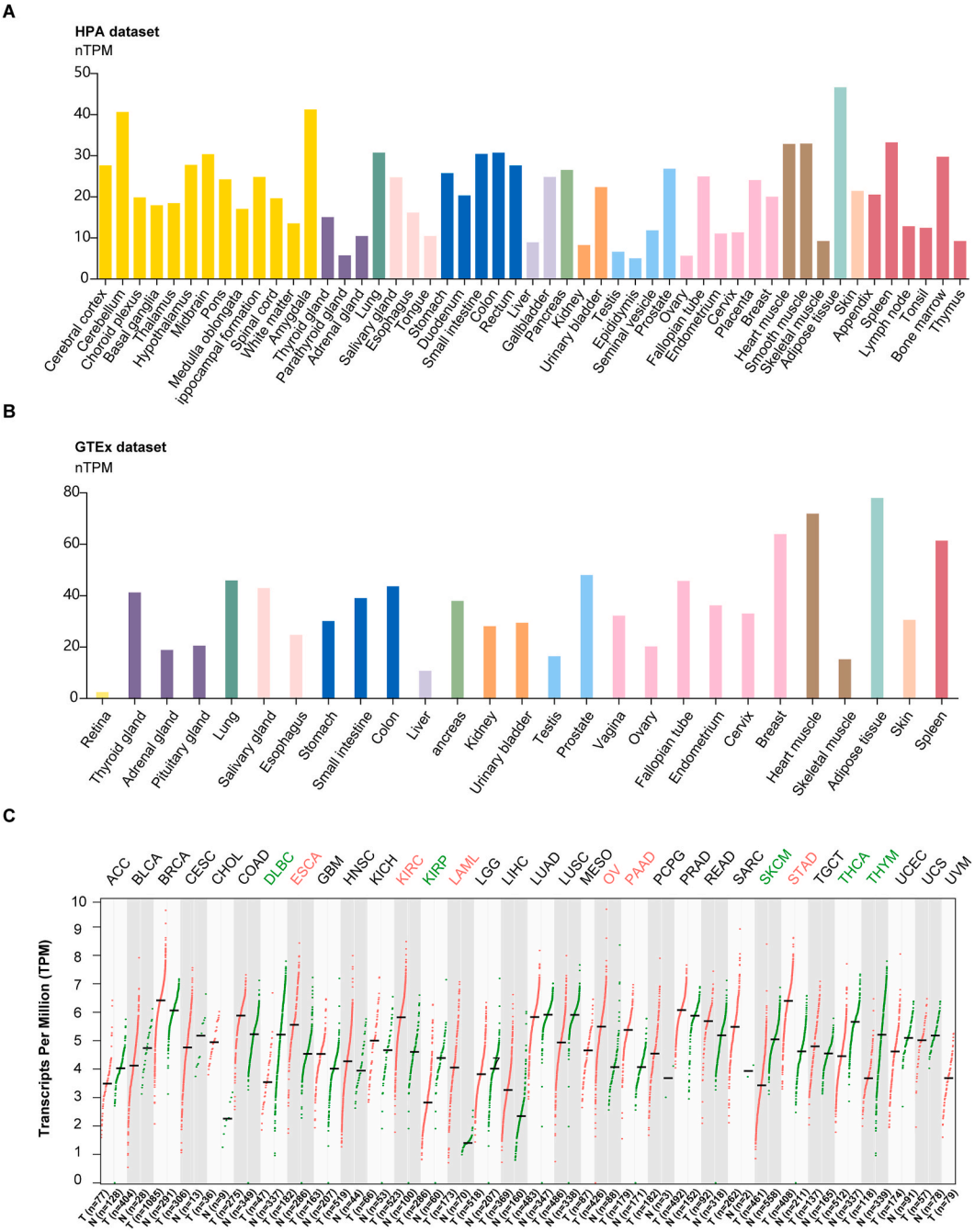

Fig. 1. The pan-cancer landscape of TP53I11 expression. (A) Using data from the HPA dataset, we analyzed the mRNA expression of TP53I11 across various human tissues. (B) The GTEx dataset provided us with information on the mRNA expression of TP53I11 in different human tissues. (C) Using the GEPIA2 web tool, we examined the mRNA expression of TP53I11 in multiple normal tissues and cancers. Columns labeled with colors signify statistically significant differences compared to normal tissues, with red indicating upregulation and green indicating downregulation.

2.15. Co-immunoprecipitation (CoIP)

To obtain whole cell extract containing stabilized F-actin, we lysed HUVECs cells at 4 °C with actin stabilizing buffer (1 % Triton-X 100, 10 mM EDTA, 0.1 % SDS, 1 % sodium deoxycholate, 50 mM NaCl, 5 mM MgCl2,1 mM ATP and 10 mM Tris-HCl, pH 7.5) supplemented with a protease inhibitor mixture (Roche, 11697498001). After centrifugation at 12000 rpm for 30min, the supernatant fraction was harvested as the total cellular protein extract and then incubated with SureBeads (BioRad, 161–4833) previously coated with anti F-actin antibody (Abcam, ab205) or control IgG antibody (Abcam, ab276304) at room temperature for 1 h protein complexes were eluted from the beads by boiling in 2x SDS-PAGE sample loading buffer for 10 min (Beyotime, P0288), and analyzed by Western blot as described above.

2.16. Luciferase reporter assays

The hypoxia response element (HRE) binding sites within a 2000 bp region upstream of the human TP53I11 sequence were scrutinized using the Jasper website [27] (http://jaspar.genereg.net/). Transcription factor sequences (HIF-1α, HIF-2α, TP53) were incorporated into the transient expression vector, pCDNA3.1. Following this, the promoter region sequences, either wild-type or mutated, spanning 2000 base pairs upstream of the TP53I11 transcription start site (TSS), were introduced upstream of the reporter vector, pGL-SV40-RLuc-△Pro-Luc vector. HEK293T cells underwent transfection with pCDNA3.1 (NC, HIF-1, HIF-2α, or TP53) alongside the luciferase plasmid driven by either the wild-type HRE promoter (wHRE) or the mutated HRE promoter (mHRE) in TP53I11. Subsequently, luciferase activity was quantified using the Dual-Lumi Luciferase Reporter Gene Assay Kit (Beyotime, China)

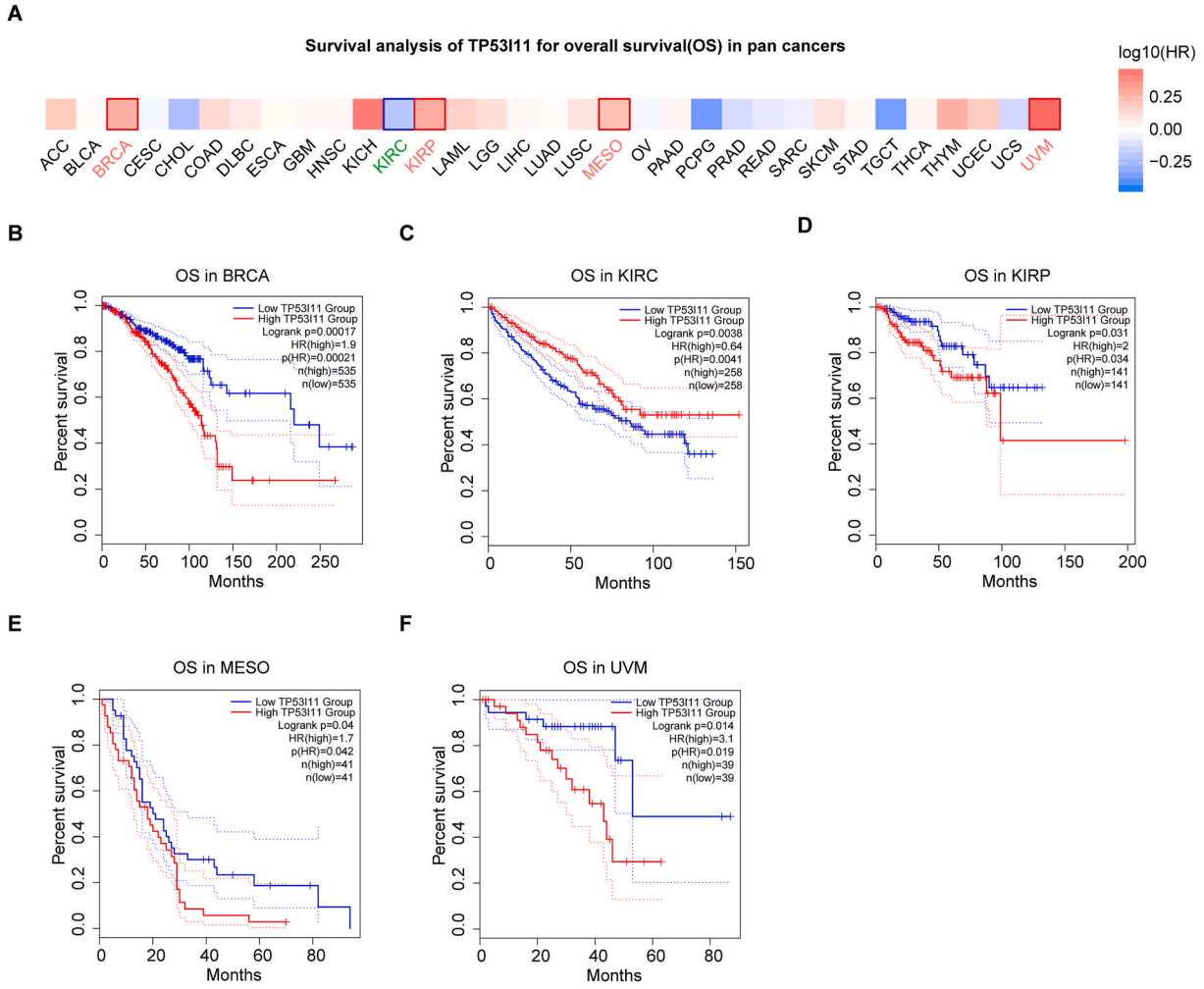

Fig. 2. Association of TP53I11 mRNA expression with overall survival (OS) in pan-cancer. (A) The GEPIA2 web tool was used to assess the prognostic significance of TP53I11 across several types of human cancers. (B–F) Kaplan-Meier survival curves were generated to compare the overall survival (OS) rates between TP53I11 high- and low-expression groups in five different types of cancers: breast invasive carcinoma (BRCA), kidney renal clear cell carcinoma (KIRC), kidney renal papillary cell carcinoma (KIRP), mesothelioma (MESO), and uveal melanoma (UVM).

on the GloMax Luminometer (Promega), following the manufacturer's instructions. Finally, data from luciferase reporter assay were analyzed based on the Renilla/firefly luciferase ratio.

2.17. Statistical analysis

Statistical analyses were conducted using R statistical package. When comparing two groups, two-tailed Student's t-test, or Mann-Whitney *U* test was employed. To determine the differences between more than two groups, one-way ANOVA with Bonferroni's post-

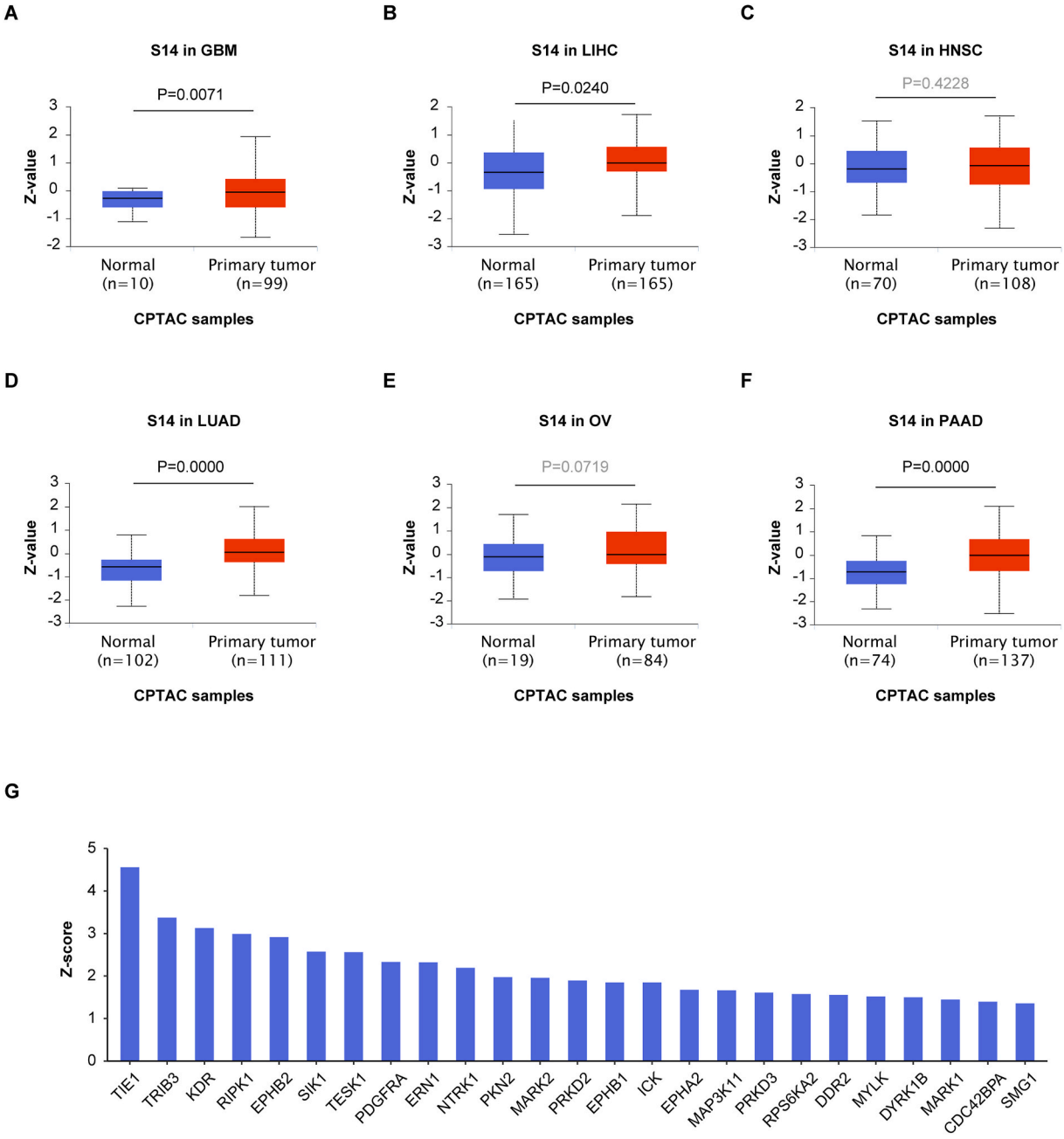

Fig. 3. Analysis of protein phosphorylation of TP53I11 in pan-caner. (A–F) The UALCAN web tool, using the CPTAC dataset, was utilized to investigate protein phosphorylation of TP53I11 across multiple cancers. Box plots were generated to display the variations in SHROOM4 phosphoprotein (specifically, phosphorylation sites S14) between normal tissue and primary tumor for (A) GBM, (B) LIHC, (C) HNSC, (D) LUAD, (E) OV, and (F) PAAD. P-values were determined via unpaired t-tests. (G) The ARCHS4 database was utilized for Kinase Enrichment Analysis (KEA) to predict the upstream kinases involved in the phosphorylation of TP53I11 protein.

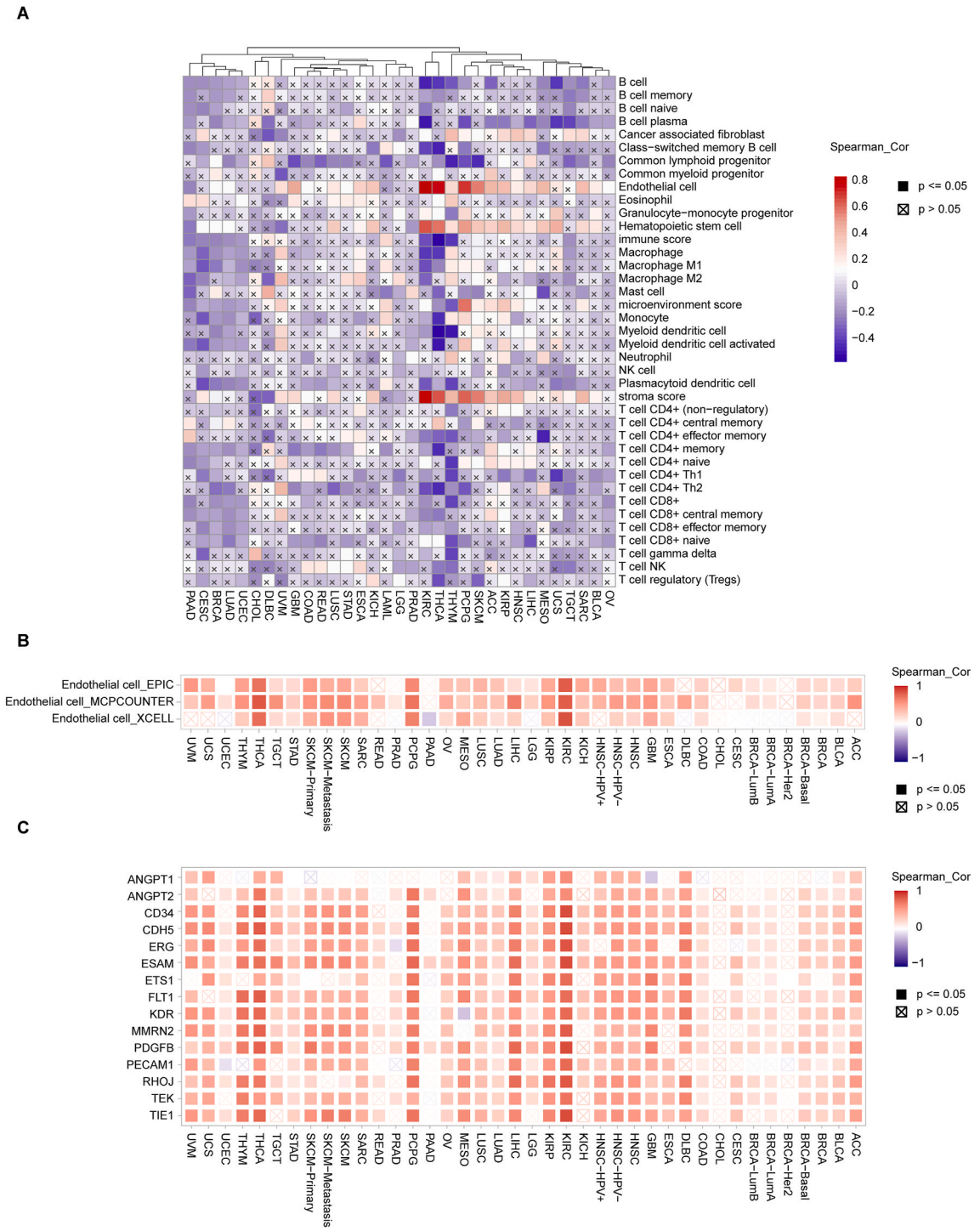

Fig. 4. TP53I11 is associated with vascular endothelial features in cancer. (A) The heatmap illustrates the correlation between TP53I11 expression and the level of immune infiltration in various cancer types, as determined by XCELL algorithms. (B) Using TIMER2 web tool based on EPIC, MCPCOUNTER, and XCELL algorithms, the heatmap displays the correlation between SHROOM4 expression and the infiltration of immune cells in ECs across different types of cancer. (C) Using TIMER2 web tool, the heatmap shows the expression correlation between TP53I11 and several known markers of vascular ECs (including ANGPT1, ANGPT2, CD34, CDH5, ERG, ESAM, ETS1, FLT1, KDR, MMRN2, PDGFB, PECAM1, RHOJ, TEK, and TIE1) in diverse cancer types.

hoc test was performed. All experiments were repeated at least three times to ensure reliability. Statistical significance was set at $P < 0.05$.

3. Results

3.1. Expression of TP53I11 in normal tissues and various cancers

The expression of TP53I11 mRNA in normal tissues was examined using the HPA database. Both the HPA and GTEx data showed that TP53I11 was expressed in a wide range of tissues and organs, including the integumentary, digestive, respiratory, genital, endocrine, urinary, nervous, musculoskeletal, cardiovascular, and immune systems (Fig. 1A and B). TP53I11 expression has low tissue specificity. To investigate the expression of TP53I11 mRNA in human cancers, we used the GEPIA2 database (accessed on February 15, 2023). A comparison of mRNA expression between tumor and normal tissues revealed that TP53I11 was abnormally expressed in many human cancer types (Fig. 1C). Notably, TP53I11 expression was significantly downregulated in five cancer types, namely, DLBC, KIRP, SKCM, THCA, and THYM, while it was significantly upregulated in six cancer types, namely, ESCA, KIRC, LAML, OV, PAAD, and STAD (Fig. 1C).

3.2. Prognostic analysis of TP53I11 expression in various cancers

The relationship between TP53I11 expression and pan-cancer prognosis was analyzed using both log-rank analysis and univariate Cox regression analysis using the GEPIA2 database. As shown in Fig. 2A, high TP53I11 expression was significantly associated with better overall survival (OS) in KIRC (HR = 0.64, p = 0.0041, Fig. 2C) and poor OS in BRCA (HR = 1.9, p = 0.0002, Fig. 2B), KIRP (HR = 2, p = 0.034, Fig. 2D), MESO (HR = 1.7, p = 0.042, Fig. 2E), and UVM (HR = 3.1, p = 0.019, Fig. 2F). As shown in Fig. S1A, high TP53I11 expression was significantly associated with better disease-free survival (DFS) in KIRC (HR = 0.7; p = 0.049, Fig. S1D) and poor DFS in ACC (HR = 2; p = 0.046, Fig. S1B), BLCA (HR = 1.4; p = 0.038, Fig. S1C), KIRP (HR = 2.2; p = 0.0087, Fig. S1E), UCEC (HR = 2; p = 0.042, Fig. S1F), and UVM (HR = 3.5; p = 0.017, Fig. S1G).

3.3. DNA methylation of TP53I11 in various cancers

DNA methylation, a process that marks changes in DNA molecules, can be dynamically altered in response to external stimuli, such as stress and dietary changes, and DNA methylation patterns can be passed down from one generation to the next. Aberrant changes in DNA methylation patterns have been linked to several types of cancer. As shown in Fig. S2A, the GSCA database revealed DNA methylation patterns of TP53I11 across 33 cancers. An inverse relationship was observed between DNA methylation and mRNA expression in most cancer types (Fig. S2B), including KIRC (Fig. S2C), LGG (Fig. S2D), and UVM (Fig. S2E). Furthermore, based on the TP53I11 DNA methylation levels, the survival curves revealed that high methylation of TP53I11 resulted in poor OS, DFS, and DSS in KIRC (Figs. S3A, S3D, and S3G), as well as better OS, DFS, and DSS in LGG (Figs. S3B, S3E, and S3H) and UVM (Figs. S3C, S3F, and S3I).

3.4. Phosphorylation of TP53I11 protein in various cancers

Phosphorylation is a post-translational modification that significantly affects protein function and activity. During phosphorylation, a phosphate group is added to the protein molecule through transfer from adenosine triphosphate (ATP) to a specific amino acid residue (phosphorylation site) on the protein. The S14 site refers to a specific serine residue, Ser14, on TP53I11 that is phosphorylated. The levels of protein phosphorylation at S14 were compared between normal and primary tumor tissues using data from the CPTAC database available on the UALCAN website. The results indicated an increase in the phosphorylation level of S14 in several cancers, including GBM (Fig. 3A), LIHC (Fig. 3B), LUAD (Fig. 3D), and PAAD (Fig. 3F). However, no significant differences were observed between HNSC (Fig. 3C) and OV (Fig. 3E). To facilitate future research, as shown in Fig. 3G, the upstream kinases of TP53I11 phosphorylation were predicted through Kinase Enrichment Analysis (KEA) using the ARCHS4 database. The upstream kinase with the highest predicted score is TIE1.

3.5. Positive correlation between TP53I11 expression and ECs in various cancers

The tumor microenvironment comprises four key elements, namely, immune, vascular, extracellular, and stromal, which facilitate communication between tumor cells and their microenvironment. As shown in Fig. 4A, the XCELL algorithm was used to analyze the correlation between TP53I11 expression and the TME components. The results showed that TP53I11 expression significantly and positively correlated with ECs, hematopoietic stem cells, and stroma scores in various cancers. Furthermore, the TIMER2 website was used to analyze the correlation between TP53I11 expression and ECs in all cancers. We obtained results using the EPIC, MCPCOUNTER, and XCELL algorithms and found that in some cancers, TP53I11 expression was positively correlated with ECs (Fig. 4B). To gather further evidence on the relationship between TP53I11 and ECs, correlation analysis was performed using the TIMER2 database and by selecting EC-specific markers, such as ANGPT1, ANGPT2, CD34, CDH5, ERG, ESAM, ETS1, FLT1, KDR, MMRN2, PDGFB, PECAM1, RHOJ, TEK, and TIE1. Our data indicated a strong positive correlation, suggesting that TP53I11 may have phenotypic characteristics similar to those of EC-specific markers (Fig. 4C).

3.6. Single-cell analysis of TP53I11 expression pattern in normal tissues and various cancers

Single-cell analysis is particularly useful for studying the molecular diversity of different cell types. First, single-cell analysis was conducted for cancer using the MMUcan and CancerSEA databases. As shown in Fig. 5A, the IMMUcan database presents a heatmap of

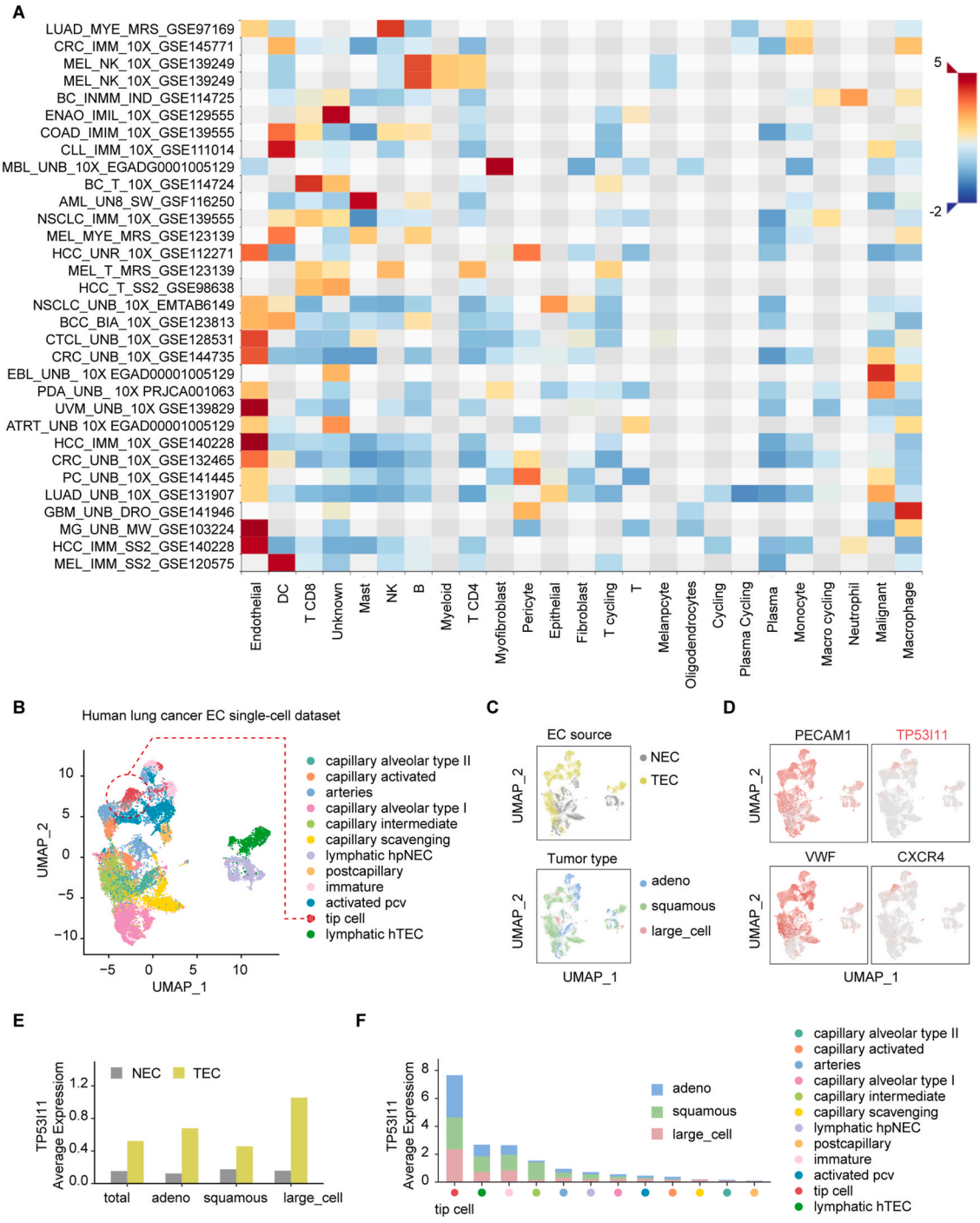

Fig. 5. Single-cell analysis of TP53I11 expression pattern in pan-cancer. (A) Single-cell analysis of TP53I11 subcellular localization in tumor microenvironment (TME) using the MMUcan database. (B–D) Clustering is conducted based on cell type (B), sources (C), and tumor types (D), visualized using the UMAP algorithm from the Lung Tumor ECTax database through the Seurat package. (E) Validation of PECAM1, VWF, CXCR4 and TP53I11 in the UMAP projection. (F) Grouped bar chart shows the expression of TP53I11 in endothelial cells across total and different lung cancer types. (G) Stacked bar chart shows the expression pattern of TP53I11 in distinct lung cancer types and varied endothelial cell subtypes.

the average expression of TP53I11 in each cell type in 32 cancer datasets, showing that TP53I11 is predominantly expressed in endothelial cells (ECs) in the tumor microenvironment. As shown in Fig. S4, the CancerSEA database revealed that TP53I11 expression in retinoblastoma (RB) was significantly positively correlated with angiogenesis and differentiation. These results suggest that

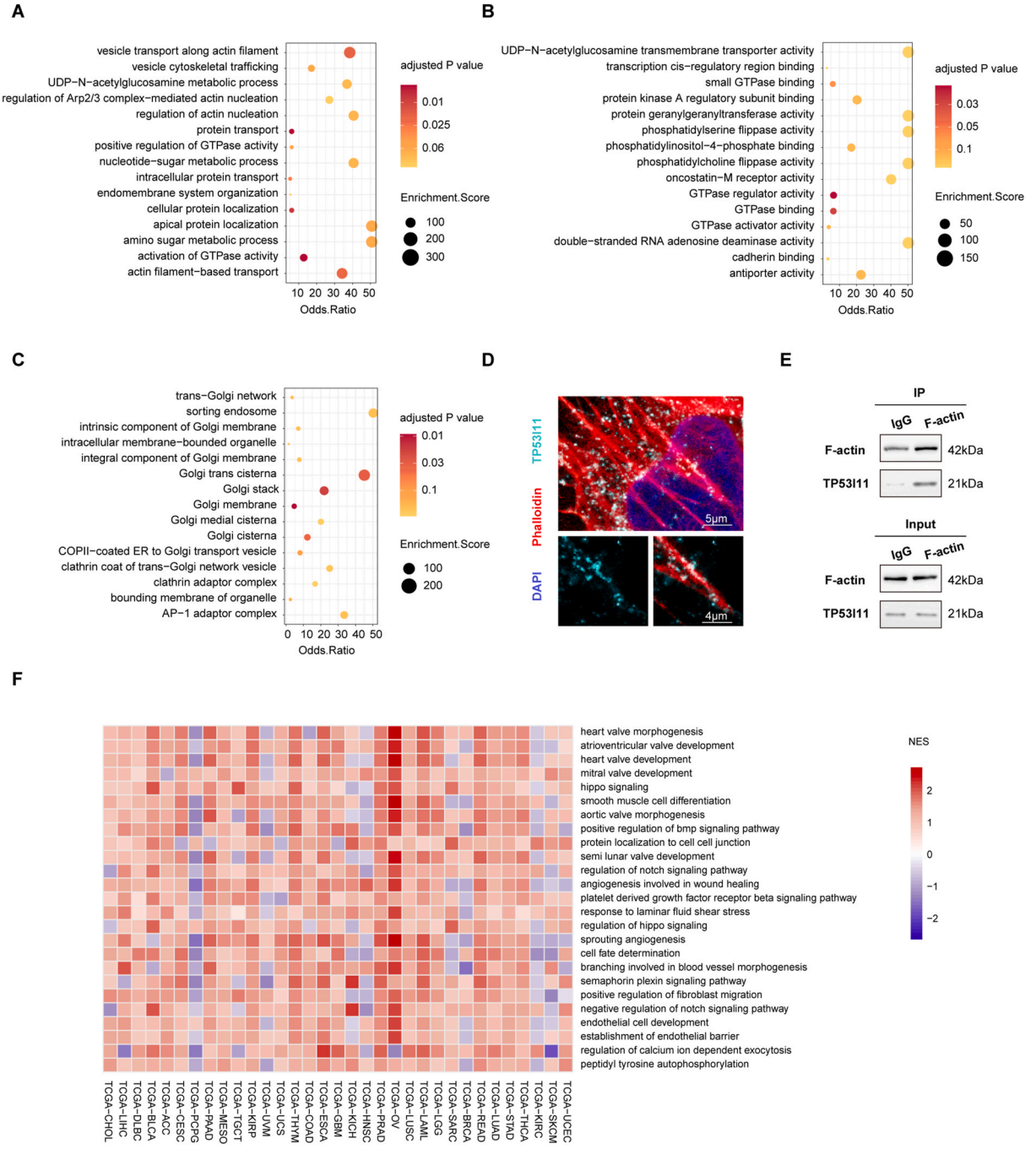

Fig. 6. TP53I11-related enrichment analysis. (A–C) We obtained the top 100 genes related to TP53I11 using the GEPIA2 web tool and conducted GO analysis on these genes for (A) biological processes, (B) molecular functions, (C) cellular components, and. (D) HUVECs were fluorescence stained for TP53I11(turquoise), F-Actin/phalloidin (red) and DAPI (blue). (E) CoIP experiments using F-actin as the bait. Representative gel of one out of three independent experiments. Protein lysates were treated with actin stabilizing buffer prior to CoIP. (F) Based on the differentially expressed genes between TP53I11 high- and low-expression groups across 33 cancers from the TCGA database, GSEA analysis shows the top 25 upregulated enriched biological processes. The enriched biological processes, ranked based on normalized enrichment score (NES), are shown in a heatmap.

TP53I11 is a novel angiogenic factor in ECs.

To elucidate the correlation between TP53I11 and vascular endothelial cells, we employed the Lung Tumor ECTax database [28], a robust resource facilitating the exploration of gene expression within endothelial cell subtypes. Utilizing the clustering and grouping annotations from the original author, we reconfigured visualizations to depict the distribution of vascular endothelial cell subtypes (Fig. 5B), categorized by both source and tumor type (Fig. 5C). To delineate the spatial distribution of TP53I11 within endothelial cell subtypes, we utilized well-established endothelial cell marker genes (PECAM1 and VWF) and tip cell marker genes (CXCR4). The results indicated a congruent distribution pattern between TP53I11 and CXCR4 (Fig. 5D). Furthermore, we conducted an in-depth exploration of TP53I11 expression in ECs across various lung cancer types. The outcomes showcased significant expression of TP53I11 in all three subtypes of lung cancer (adenocarcinoma, large-cell carcinoma, and squamous cell carcinoma), as well as in the overall lung cancer patient cohort (Fig. 5E), with the apex of expression observed in tip cells (Fig. 5F).

Next, a single-cell analysis was performed using the EC Atlas and Murine ECTax database for several normal murine tissues. According to the two-dimensional diagrams in Fig. S5, TP53I11 is expressed in ECs across various tissues, including the brain, colon, extensor digitorum longus (EDL), heart, kidney, liver, lung, small intestine, soleus, spleen, testis, and choroid. Its expression in ECs is particularly pronounced in the colon (Fig. S5B), heart (Fig. S5D), soleus (Fig. S4I), spleen (Fig. S5J), and choroid (Fig. S5L), while being

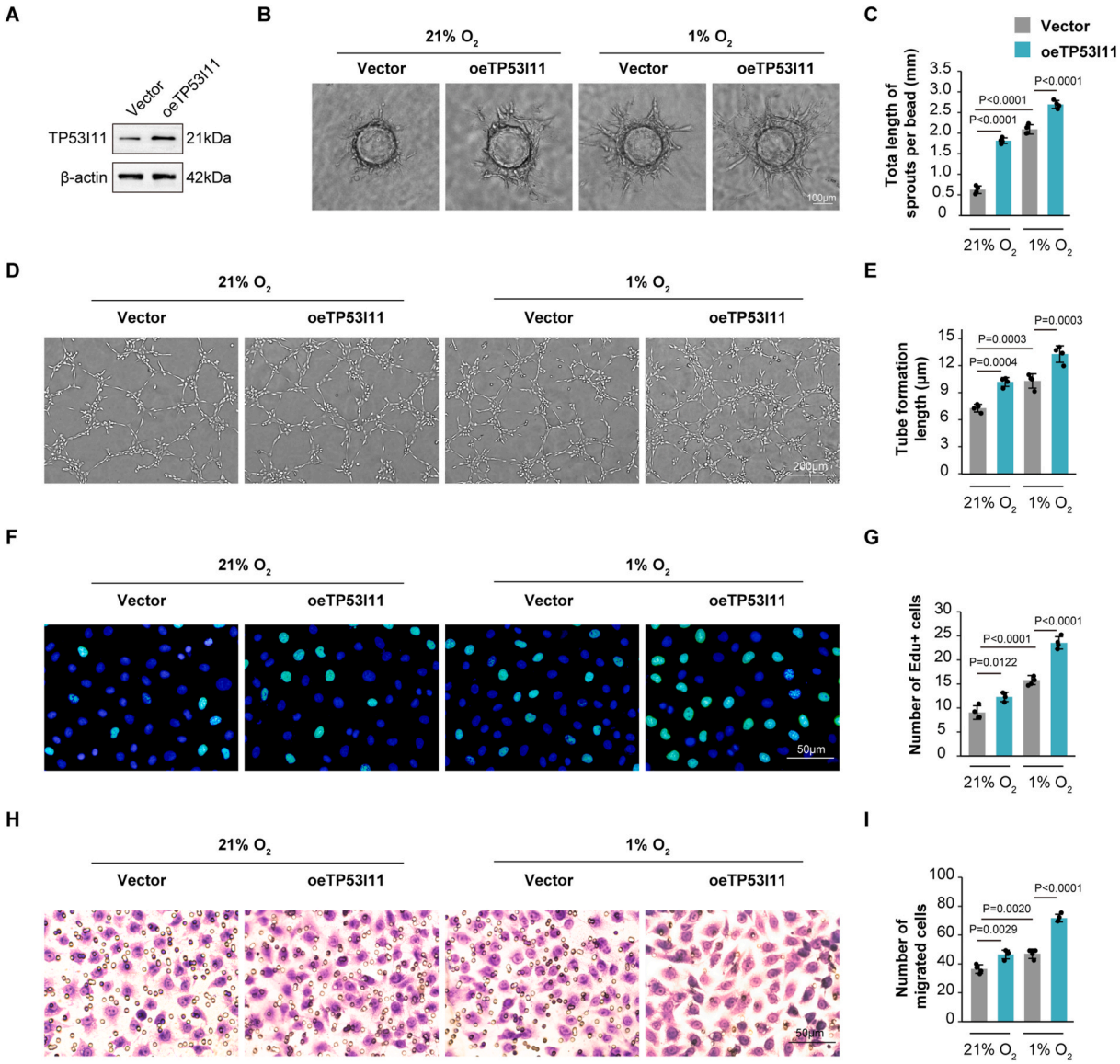

Fig. 7. Validation of angiogenic function of TP53I11 in vitro. (A) Western blot of TP53I11 in HUVECs transfected with TP53I11 overexpression plasmids (oeTP53I11) and a mock control (vector). (B–I) The micro-vessel sprouting, tube formation, proliferative, and migratory abilities of cells in each group were evaluated using the fibrin bead angiogenesis assay, tube formation assay, EdU assay, and Transwell assay, respectively (n = 4 samples for each group). Error bars represent mean ± SEM; One-way ANOVA with Bonferroni's post hoc test (C, E, G, I).

comparatively lower in the brain (Fig. S5A), kidney (Fig. S5E), and lung (Fig. S5G). These findings strongly suggest a notable connection between TP53I11 and endothelial cells, particularly tip cells, implying a potential impact on their physiological or pathological functions.

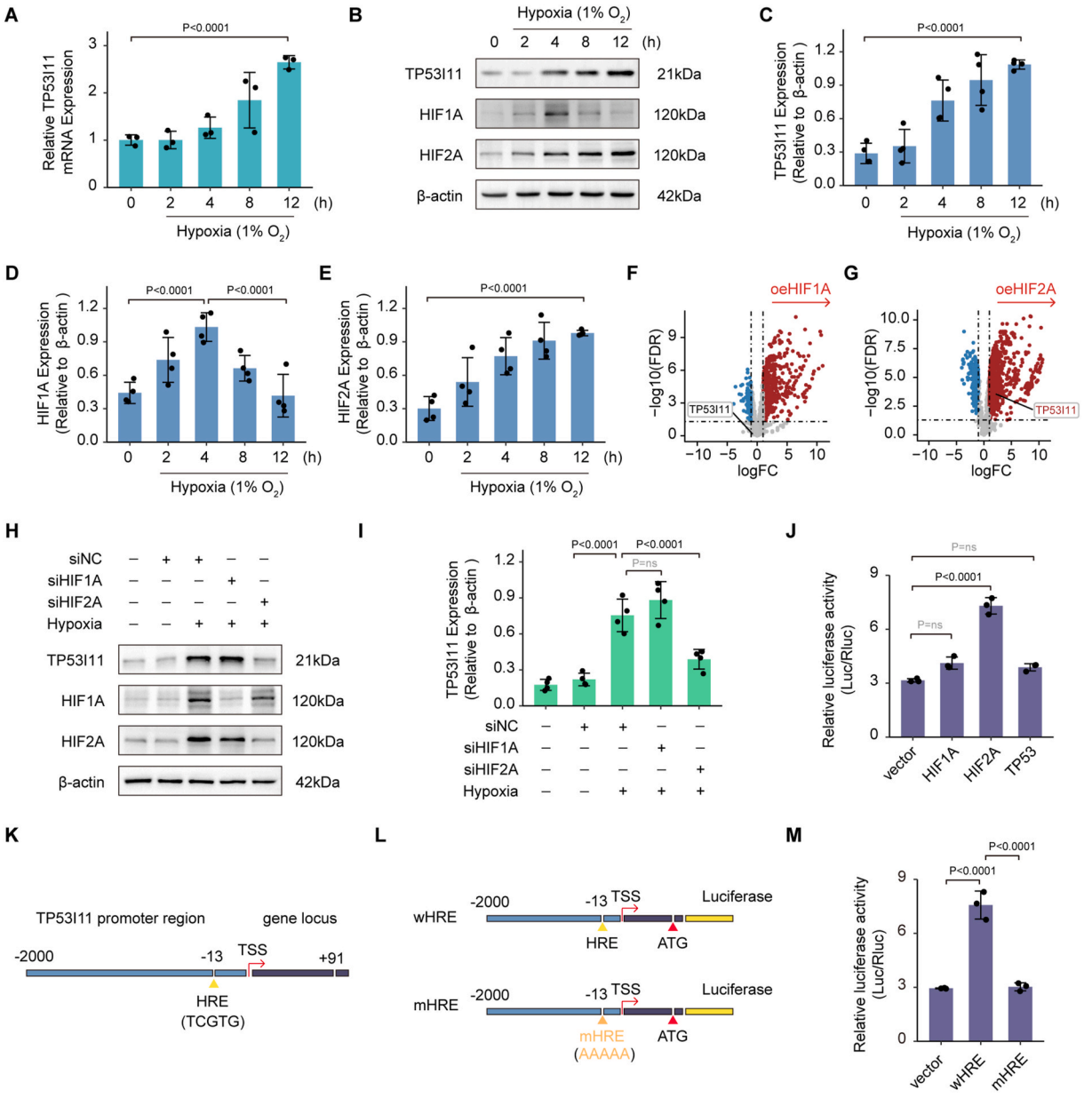

Fig. 8. HIF-2α upregulates TP53I11 expression upon hypoxia in ECs. (A) TP53I11 mRNA levels were assessed in endothelial cells (ECs) subjected to hypoxic conditions (1 % O_2) for the specified durations (n = 4 independent experiments). (B–E) Western blot analysis and the quantitation of TP53I11, HIF-1α, and HIF-2α proteins was conducted in ECs exposed to hypoxia (1 % O_2) for the indicated time points (n = 4 independent experiments). (F–G) Volcano plots for the overexpression of either HIF-1α or HIF-2α in HUVECs. (H–I) Western blot analysis and quantitation of TP53I11, HIF-1α, and HIF-2α proteins were conducted in ECs either untreated or exposed to hypoxia (1 % O_2) for 4 h, along with transfection using siNC, siHIF-1α, or siHIF-2α (n = 4 independent experiments). (J) Luciferase reporter assays were performed to evaluate TP53I11 promoter activity in HEK293T cells transfected with control vector, HIF-1α overexpression, or HIF-2α overexpression plasmids (n = 3 independent experiments). (K) A diagrammatic representation of hypoxia response element (HRE) sequences in the human TP53I11 promoter was derived from the JASPAR database. (L) A schematic diagram depicting mutated HRE (mHRE) introduced into the human TP53I11 promoter. (M) Luciferase reporter assays were conducted to assess TP53I11 promoter activity in HEK293T cells following transfection of wild-type HRE (wHRE) or mHRE vectors under HIF-2α overexpression (n = 3 independent experiments). Error bars represent mean ± SEM; One-way ANOVA with Bonferroni's post hoc test (A, C, D, E, I, J, M). TSS, transcription start site.

3.7. Enrichment analysis of TP53I11 in various cancers

To investigate the possible mechanisms underlying the role of TP53I11 in pan-cancer, we analyzed the top 100 genes that exhibited expression patterns similar to those of TP53I11, as shown in Table S1. GO analyses were performed. The results of the BP analysis showed significantly related biological processes, including vesicle transport along actin filaments, actin filament-based transport, regulation of actin nucleation, apical protein localization, amino sugar metabolic processes, and activation of GTPase activity (Fig. 6A). MF showed significantly related molecular functions, including GTPase regulatory activity and GTPase binding (Fig. 6B). The CC results showed significantly related cellular components, including the Golgi *trans*-cisterna, Golgi stack, Golgi membrane, and Golgi cisterna (Fig. 6C). An immunofluorescence assay revealed the co-localization of TP53I11 with the actin cytoskeleton, indicating a possible interaction between TP53I11 and the actin cytoskeleton (Fig. 6D). Besides, actin binding of TP53I11 was verified by co-immunoprecipitation (CoIP) from HUVECs cellular extracts (Fig. 6E).

Next, GSEA was conducted across 33 cancer types, utilizing the differential expression patterns of the TP53I11 gene between the high- and low-expression groups for each type of cancer. A heatmap was used to display the 25 most enriched biological processes sorted by their normalized enrichment score (NES) (Fig. 6F). The GSEA result showed that TP53I11 high expression group had good enrichment score and significance in heart valve morphogenesis, Hippo signaling, positive regulation of BMP signaling pathway, protein localization of cell-cell junction, regulation of Notch signaling pathway, angiogenesis involved in wound healing, sprouting angiogenesis, branching involved in blood vessel morphogenesis, platelet-derived growth factor receptor beta (PDGFB) signaling pathway, semaphoring-plexin signaling pathway, positive regulation of fibroblast migration, EC development, establishment of endothelial barrier, and regulation of calcium ion-dependent exocytosis (Fig. 6F).

Additionally, ARCHS4 database predicted the function of TP53I11, including in endothelium development, vascular endothelial growth factor signaling pathway, semaphoring-plexin signaling pathway, cellular response to vascular endothelial growth factor stimulus, and basement membrane organization, as well as possible KEGG pathways, including Notch signaling pathway and axon guidance (Fig. S6).

3.8. TP53I11 affects endothelial cell function in vitro

To validate the angiogenic role of TP53I11 in ECs, in vitro angiogenesis assays were conducted using HUVECs. HUVECs were transfected with the TP53I11 overexpression plasmid, and the transfection efficiency was assessed by eGFP (approximately 75 %, Fig. S7). As demonstrated in Fig. 7A, Western blot revealed the successful transfection of the TP53I11 overexpression plasmid into HUVECs. Through in vitro angiogenesis assays, we found that exposure to hypoxia in vitro had the potential to enhance the angiogenic capacity of endothelial cells (Fig. 7B–I). We observed that overexpression of TP53I11 significantly increased microvessel sprouting (Fig. 7B–C), tube formation (Fig. 7D–E), proliferation (Fig. 7F–G), and migration (Fig. 7H–I) in HUVECs under normoxia or hypoxia condition.

Furthermore, we generated a lentiviral CRISPR/Cas9 knockout of TP53I11 in HUVECs to enhance understanding of TP53I11 function. The knockout efficiency was confirmed by Western blot analysis (Fig. S8A). Among the generated knockout lines, koTP53I11 #1 exhibited a superior knockout effect (Fig. S8A). Contrary to the results observed with TP53I11 overexpression, the knockout of TP53I11 significantly attenuated microvessel sprouting (Figs. S8B–C), tube formation (Figs. S8D–E), proliferation (Figs. S8F–G), and migration (Figs. S8H–I) in HUVECs under both normoxic and hypoxic conditions. These experimental findings align with conclusions drawn from bioinformatic analysis, collectively suggesting that TP53I11 plays a crucial role in angiogenesis.

3.9. TP53I11 is transcriptionally up-regulated by HIF2A under hypoxia

Hypoxia in the tumor microenvironment (TME) acts as a potent catalyst for tumor angiogenesis [29]. We aimed to investigate whether hypoxia induces alterations in TP53I11 expression. Our observations unveiled a progressive increase in both TP53I11 mRNA and protein levels with extended hypoxic exposure (Fig. 8A–C). Notably, a similar trend was noted compared to that of HIF-2α (Fig. 8B–E). We hypothesize that HIF-2α may serve as an upstream inducer of TP53I11 transcription.

To validate these hypotheses, initially, we utilized publicly accessible data from the GEO database (GSE98060) [30]. This dataset involved RNA-seq on HUVECs subjected to overexpression of either HIF-1α or HIF-2α. The volcano plot analysis indicated a significant upregulation of TP53I11 mRNA expression in HUVECs with HIF-2α overexpression (p-value <0.05, log2FoldChange $= 1.497$), in contrast to HIF-1α overexpression (Fig. 8F–G). To assess whether HIF-2α is crucial for TP53I11 expression, we utilized siRNA to silence HIF-2α expression following a 4-h hypoxic treatment. Our findings demonstrated that IRF1 siRNA treatment blunted the induction of TP53I11 upon hypoxia stimulation, while the knockdown of HIF-1α had no impact (Fig. 8H–I). Furthermore, the Luciferase reporter assay illustrated that the HIF-2α transcription factor enhanced the activity of the TP53I11 promoter, while HIF-1α and TP53 transcription factors showed no significant impact (Fig. 8J). Additionally, using the JASPAR database, we identfied a singular hypoxia response element (HRE) site (5′-TCGTG-3′, 13bp relative to the TSS) and mutated it (Fig. 8K-L). The Luciferase reporter assay revealed that the mutation disrupted the transcriptional activation effect of HIF-2α (Fig. 8M). In summary, it can be concluded that in endothelial cells, HIF-2α is the key mediating factor in the hypoxia-induced elevation of TP53I11 expression levels.

4. Discussion

It is important to understand the role of angiogenesis in tumor development because malignant tumors require a constant supply of

oxygen and nutrients to survive and grow [31]. The initiation of tumor angiogenesis is a crucial factor in this process, as it allows the tumor to access the bloodstream and receive essential supplies [32]. Several angiogenic factors have been identified, and their inhibitors, shown to be effective in cancer treatment, have been developed [33,34]. Hence, to tackle cancer more effectively and understand tumor growth, it is crucial to have a thorough understanding of angiogenesis in relation to cancer.

The discovery of TP53I11 dates back over 20 years; however, limited information is available regarding its structure and function. To our knowledge, this is the first report to identify the angiogenic role of TP53I11 in cancer. Several studies have suggested that TP53I11 plays an important role in angiogenesis. Due to recent rapid progress in single-cell sequencing technology, multiple bioinformatic studies have predicted the discovery of a novel EC marker, TP53I11, expressed in the tip cells of the vascular endothelium [35,36].Through bioinformatics analysis of lung cancer, our study yielded identical conclusions. During angiogenesis, tip cells initiate the formation of new vessels by sprouting from existing vessels and forming the leading edge of the sprout [37].Thus, it is not surprising that TP53I11 participates in cancer angiogenesis.

The genomic characteristics of TP53I11 have not been described in pan-cancer analyses. Elevated TP53I11 expression has been detected in several cancer types, including ESCA, KIRC, LAML, OV, PAAD, and STAD, indicating its potential role in cancer initiation and progression. Moreover, high TP53I11 expression levels have been linked to poor outcomes in patients with tumors, such as BRCA, MESO, ACC, BLCA, KIRP, UCEC, and UVM. However, notably, KIRC exhibited a more favorable prognosis. Che et al. conducted bioinformatics research to explore the relationship between angiogenesis-related genes and KIRC [28]. They observed that, unlike in other tumors (such as UCEC and KICH), most angiogenesis-related genes in patients with KIRC acted as protective factors [28]. This suggests that the data for KIRC may be unique, although the reasons for this phenomenon remain unclear. Considering the correlation between TP53I11 and angiogenesis uncovered in this study, it is plausible that this association contributes to the observed more favorable prognosis in KIRC.

DNA methylation is an epigenetic modification that involves the covalent addition of a methyl group (-CH3) to the cytosine residues of DNA [38]. This modification can regulate gene expression by blocking the access of the transcriptional machinery to the underlying DNA sequence [39], thereby preventing the transcription of genes into RNA and the subsequent synthesis of protein products. In accordance with the repression of transcription through DNA methylation, we found a significant inverse relationship between DNA methylation and gene expression of TP53I11 across most cancer types. We also found that patients with KIRC presented a better prognosis with TP53I11 hypomethylation, whereas patients with LGG and UVM showed a better prognosis with TP53I11 hypermethylation. These findings suggest that TP53I11 may serve as a predictive marker for the prognosis of patients with tumors.

Phosphorylation is the post-translational modification of proteins in which a phosphate group is added to a specific amino acid residue in the protein molecule [40]. Although TP53I11 phosphorylation has not been reported, a significant enhancement was found in pan-cancer; the S14 site was phosphorylated in multiple cancer types, including GBM, LIHC, LUAD, and PAAD. Phosphorylation may lead to changes in activity, localization, and interactions of modified proteins, and in turn, may regulate various cellular processes, such as gene expression, cell division, and metabolism [41]. Thus, phosphorylated TP53I11 is hypothesized to be the active form of the angiogenic factor. However, this warrants further investigation for corroborative elucidations.

The role of ECs in cancer biology is to supply tumors with vital nutrients and oxygen and serve as pathways for the spread of cancer cells [42,43]. This ultimately contributes to tumor progression. Single-cell analysis revealed that TP53I11 was mainly expressed in the ECs of various cancers and normal tissues. Immune cell infiltration analysis revealed that TP53I11 expression was strongly and positively correlated with EC infiltration. We also observed a significant positive association between TP53I11 and multiple EC-specific pan-cancer markers. Our study demonstrates that ECs actively produce the TP53I11 protein and, therefore, play a significant role in cellular processes.

To further identify the main role of TP53I11, a functional enrichment analysis was performed to reveal its biological processes (BP), molecular functions (MF), cellular components (CC), and pathways. 1) In angiogenesis, small sprouts are formed from the ECs of preexisting blood vessels and migrate to the site of angiogenesis [44]. These sprouts then differentiate, branch, and form new blood vessels, which eventually mature and stabilise via endothelial barrier formation [45]. BP results, such as angiogenesis involved in wound healing, sprouting angiogenesis, branching involved in blood vessel morphogenesis, EC development, and the establishment of an endothelial barrier, were correlated with angiogenesis. 2) Actin filaments—key elements of the cytoskeleton—are vital for numerous cellular processes related to angiogenesis, including vesicle transport, cell shape, movement, and division, as they constantly assemble and disassemble dynamically [46]. The BP results, such as vesicle transport along actin filaments, actin filament-based transport, and regulation of actin nucleation, were correlated with actin filament activity. Immunofluorescence and co-immunoprecipitation also confirmed that TP53I11 exhibits a binding affinity for actin, suggesting that TP53I11 may play a role in the development of blood vessels by modulating the actin cytoskeleton. 3) In angiogenesis, GTPases play a key role in regulating the migration and proliferation of ECs. For example, the Rho GTPase family, which includes RhoA, Rac1, and Cdc42, regulates the formation of filopodia and lamellipodia and promotes cell migration and proliferation [47,48]. MF results, such as GTPase regulator activity and GTPase binding, were correlated with GTPase activity, suggesting that the TP53I11 protein may participate in angiogenesis by controlling the activity of GTPases. 4) The HPA database provided evidence that TP53I11 is located within the Endoplasmic Reticulum and Golgi Apparatus [15]. CC results, such as Golgi *trans*-cisterna, Golgi stack, Golgi membrane, and Golgi cisterna, were consistent with the results from the HPA database. (5) During sprouting angiogenesis, multiple signalling pathways are activated, including the Hedgehog [49], Notch [30], Hippo [50], and PDGFB [51] signalling pathways. These signalling pathways trigger a series of events that promote sprouting angiogenesis, such as the proliferation and migration of ECs, formation of tip cells, and the recruitment and maturation of pericytes [30,49–51]. The TP53I11 gene is believed to play a crucial role in angiogenesis, as indicated by the pathway results, and participates in various signalling pathways, such as Hedgehog, Notch, Hippo, and PDGFB. Overall, these results suggest that TP53I11 actively participates in the angiogenic activity of ECs.

We verified the impact of TP53I11 on endothelial cell function using in vitro angiogenesis assays. It is worth noting that overexpression of TP53I11 in HUVECs led to a significant increase in proliferation, migration, tube formation, and micro-vessel sprouting. These effects were also observed under hypoxic conditions. Knocking out TP53I11 in HUVECs manifests an opposing impact to that mentioned above. Additionally, we demonstrated that TP53I11 increases in response to hypoxic conditions. As reported by Zhao et al., during hypoxic stress induced by anti-angiogenic drug therapy, TP53I11 exhibits elevated expression levels in vascular endothelial cells [52]. This discovery provides additional substantiation for the regulatory effect of hypoxia on TP53I11 expression. Hypoxia-inducible factors (HIFs) represent pivotal helix-loop-helix-PAS domain transcription factors that play a crucial role in cellular responses to hypoxia [53]. A considerable body of evidence suggests that the inhibition of either HIF-1α or HIF-2α can impede the formation of tumor blood vessels [29,54]. In our study, we unveiled that HIF-2α stimulates enhanced TP53I11 expression by directly binding to the TP53I11 promoter, thereby facilitating angiogenesis. Consequently, the interaction between HIF-2α and TP53I11 further underscores TP53I11 as a pivotal regulatory factor with broad implications in hypoxia-induced angiogenesis. Further investigation is required to elucidate the downstream mechanisms through which TP53I11 promotes angiogenesis.

Our study's limitation includes the use of immortalized ECs and lack of animal experiment. Primary EC models closely resemble tissue compared to immortalized lines but face challenges like limited lifespan, low transfection, and contamination risks. Immortalized ECs may exhibit variable phenotypes due to immortalization, genetic instability, and loss of differentiation potential. Our study provides initial insights into the angiogenic role of TP53I11. Further elucidation of these observations necessitates the undertaking of comprehensive animal experiments.

In conclusion, our comprehensive pan-cancer analysis of TP53I11 revealed a strong association and predictive value for TP53I11 expression in different human cancer types. As TP53I11 expression is upregulated in multiple cancers and associated with worse outcomes, it may represent a promising target for cancer therapy. Furthermore, our findings shed light on the significant involvement of TP53I11 in angiogenesis in the tumor microenvironment, suggesting a potential mechanism by which TP53I11 expression affects the angiogenic activity of ECs in cancer. Hence, a conclusive elucidation necessitates future studies specifically focusing on TP53I11 expression and its mechanism in relation to angiogenesis.

Funding

This study was funded by the National Natural Science Foundation of China (Grant No. 82070983 and 81870679 to QJ，Grant No. 82171080 to K-RL).

Data availability statement

The original contributions presented in the study are included in the article/Supplementary Materials, further inquiries can be directed to the corresponding author.

CRediT authorship contribution statement

Wen Bai: Writing – original draft, Visualization, Methodology, Data curation. **Jun-Song Ren:** Writing – original draft, Validation. **Ke-ran Li:** Writing – review & editing, Supervision, Funding acquisition. **Qin Jiang:** Writing – review & editing, Supervision, Funding acquisition.

Declaration of competing interest

The authors declare that they have no known competing financial interests or personal relationships that could have appeared to influence the work reported in this paper.

Acknowledgments

The authors express their gratitude to the public databases TCGA, GTEx, HPA, GEPIA2, GSCA, CPTAC, IMMUcan, CancerSEA, SCEA, TIMER2, Murine ECTax, Lung Tumor ECTax, ARCHS4 and JASPER database. The authors would like to thank Editage (www.editage.cn) for English language editing.

Appendix A. Supplementary data

Supplementary data to this article can be found online at https://doi.org/10.1016/j.heliyon.2024.e29504.

References

[1] F.S. Collins, V.A. McKusick, Implications of the human genome project for medical science, JAMA 285 (2001) 540–544.
[2] D.A. Wheeler, L. Wang, From human genome to cancer genome: the first decade, Genome Res. 23 (2013) 1054–1062.

[3] N. Cancer Genome Atlas Research, J.N. Weinstein, E.A. Collisson, G.B. Mills, K.R. Shaw, B.A. Ozenberger, K. Ellrott, I. Shmulevich, C. Sander, J.M. Stuart, The cancer genome atlas pan-cancer analysis project, Nat. Genet. 45 (2013) 1113–1120.

[4] I.T.P.-C.A.o.W.G. Consortium, Pan-cancer analysis of whole genomes, Nature 578 (2020) 82–93.

[5] J.P. Lloyd, M.B. Soellner, S.D. Merajver, J.Z. Li, Impact of between-tissue differences on pan-cancer predictions of drug sensitivity, PLoS Comput. Biol. 17 (2021) e1008720.

[6] E. Pleasance, A. Bohm, L.M. Williamson, J.M.T. Nelson, Y. Shen, M. Bonakdar, E. Titmuss, V. Csizmok, K. Wee, S. Hosseinzadeh, C.J. Grisdale, C. Reisle, G. A. Taylor, E. Lewis, M.R. Jones, D. Bleile, S. Sadeghi, W. Zhang, A. Davies, B. Pellegrini, T. Wong, R. Bowlby, S.K. Chan, K.L. Mungall, E. Chuah, A.J. Mungall, R. A. Moore, Y. Zhao, B. Deol, A. Fisic, A. Fok, D.A. Regier, D. Weymann, D.F. Schaeffer, S. Young, S. Yip, K. Schrader, N. Levasseur, S.K. Taylor, X. Feng, A. Tinker, K.J. Savage, S. Chia, K. Gelmon, S. Sun, H. Lim, D.J. Renouf, S.J.M. Jones, M.A. Marra, J. Laskin, Whole-genome and transcriptome analysis enhances precision cancer treatment options, Ann. Oncol. 33 (2022) 939–949.

[7] S.L. Ricketts, J.C. Carter, W.B. Coleman, Identification of three 11p11.2 candidate liver tumor suppressors through analysis of known human genes, Mol. Carcinog. 36 (2003) 90–99.

[8] K. Polyak, Y. Xia, J.L. Zweier, K.W. Kinzler, B. Vogelstein, A model for p53-induced apoptosis, Nature 389 (1997) 300–305.

[9] J. Gu, S. Zhang, X. He, S. Chen, Y. Wang, High expression of PIG11 correlates with poor prognosis in gastric cancer, Exp. Ther. Med. 21 (2021) 249.

[10] X.M. Liu, X.F. Xiong, Y. Song, R.J. Tang, X.Q. Liang, E.H. Cao, Possible roles of a tumor suppressor gene PIG11 in hepatocarcinogenesis and As2O3-induced apoptosis in liver cancer cells, J. Gastroenterol. 44 (2009) 460–469.

[11] Y. Wang, X. Liu, G. Liu, X. Wang, R. Hu, X. Liang, PIG11 over-expression predicts good prognosis and induces HepG2 cell apoptosis via reactive oxygen species-dependent mitochondrial pathway, Biomed. Pharmacother. 108 (2018) 435–442.

[12] H. Yuan, M. Yan, G. Zhang, W. Liu, C. Deng, G. Liao, L. Xu, T. Luo, H. Yan, Z. Long, A. Shi, T. Zhao, Y. Xiao, X. Li, CancerSEA: a cancer single-cell state atlas, Nucleic Acids Res. 47 (2019) D900–D908.

[13] T. Xiao, Z. Xu, Y. Zhou, H. Zhang, J. Geng, Y. Liang, H. Qiao, G. Suo, Loss of TP53I11 enhances the extracellular Matrix-independent survival by promoting activation of AMPK, IUBMB Life 71 (2019) 183–191.

[14] S. Mamoor, Differential Expression of P53 Inducible Protein 11 (TP53I11) in Cancers of the Breast, 2021.

[15] M. Uhlen, L. Fagerberg, B.M. Hallstrom, C. Lindskog, P. Oksvold, A. Mardinoglu, A. Sivertsson, C. Kampf, E. Sjostedt, A. Asplund, I. Olsson, K. Edlund, E. Lundberg, S. Navani, C.A. Szigyarto, J. Odeberg, D. Djureinovic, J.O. Takanen, S. Hober, T. Alm, P.H. Edqvist, H. Berling, H. Tegel, J. Mulder, J. Rockberg, P. Nilsson, J.M. Schwenk, M. Hamsten, K. von Feilitzen, M. Forsberg, L. Persson, F. Johansson, M. Zwahlen, G. von Heijne, J. Nielsen, F. Ponten, Proteomics. Tissue-based map of the human proteome, Science 347 (2015) 1260419.

[16] G.T. Consortium, D.A. Laboratory, G. Coordinating Center -Analysis Working, G. Statistical Methods groups-Analysis Working, G.g. Enhancing, N.I.H.C. Fund, Nih/Nci, Nih/Nhgri, Nih/Nimh, Nih/Nida, N. Biospecimen Collection Source Site, R. Biospecimen Collection Source Site, V. Biospecimen Core Resource, B. Brain Bank Repository-University of Miami Brain Endowment, M. Leidos Biomedical-Project, E. Study, I. Genome Browser Data, E.B.I. Visualization, I. Genome Browser Data, U.o.C.S.C. Visualization-Ucsc Genomics Institute, a. Lead, D.A. Laboratory, C. Coordinating, N.I.H.p. management, c. Biospecimen, Pathology, Q. T.L. Battle, C.D. Brown, B.E. Engelhardt, S.B. Montgomery, Genetic effects on gene expression across human tissues, Nature 550 (2017) 204–213.

[17] C.J. Liu, F.F. Hu, G.Y. Xie, Y.R. Miao, X.W. Li, Y. Zeng, A.Y. Guo, GSCA: an integrated platform for gene set cancer analysis at genomic, pharmacogenomic and immunogenomic levels, Briefings Bioinf. 24 (2023).

[18] A. Lachmann, D. Torre, A.B. Keenan, K.M. Jagodnik, H.J. Lee, L. Wang, M.C. Silverstein, A. Ma'ayan, Massive mining of publicly available RNA-seq data from human and mouse, Nat. Commun. 9 (2018) 1366.

[19] J. Camps, F. Noel, R. Liechti, L. Massenet-Regad, S. Rigade, L. Gotz, C. Hoffmann, E. Amblard, M. Saichi, M.M. Ibrahim, J. Pollard, J. Medvedovic, H.G. Roider, V. Soumelis, Meta-analysis of human cancer single-cell RNA-seq datasets using the IMMUcan database, Cancer Res. 83 (2023) 363–373.

[20] J. Kalucka, L. de Rooij, J. Goveia, K. Rohlenova, S.J. Dumas, E. Meta, N.V. Conchinha, F. Taverna, L.A. Teuwen, K. Veys, M. Garcia-Caballero, S. Khan, V. Geldhof, L. Sokol, R. Chen, L. Treps, M. Borri, P. de Zeeuw, C. Dubois, T.K. Karakach, K.D. Falkenberg, M. Parys, X. Yin, S. Vinckier, Y. Du, R.A. Fenton, L. Schoonjans, M. Dewerchin, G. Eelen, B. Thienpont, L. Lin, L. Bolund, X. Li, Y. Luo, P. Carmeliet, Single-cell transcriptome atlas of murine endothelial cells, Cell 180 (2020) 764–779 e720.

[21] K. Rohlenova, J. Goveia, M. Garcia-Caballero, A. Subramanian, J. Kalucka, L. Treps, K.D. Falkenberg, L. de Rooij, Y. Zheng, L. Lin, L. Sokol, L.A. Teuwen, V. Geldhof, F. Taverna, A. Pircher, L.C. Conradi, S. Khan, S. Stegen, D. Panovska, F. De Smet, F.J.T. Staal, R.J. McLaughlin, S. Vinckier, T. Van Bergen, N. Ectors, P. De Haes, J. Wang, L. Bolund, L. Schoonjans, T.K. Karakach, H. Yang, G. Carmeliet, Y. Liu, B. Thienpont, M. Dewerchin, G. Eelen, X. Li, Y. Luo, P. Carmeliet, Single-cell RNA sequencing maps endothelial metabolic plasticity in pathological angiogenesis, Cell Metabol. 31 (2020) 862–877 e814.

[22] J. Goveia, K. Rohlenova, F. Taverna, L. Treps, L.C. Conradi, A. Pircher, V. Geldhof, L. de Rooij, J. Kalucka, L. Sokol, M. Garcia-Caballero, Y. Zheng, J. Qian, L. A. Teuwen, S. Khan, B. Boeckx, E. Wauters, H. Decaluwe, P. De Leyn, J. Vansteenkiste, B. Weynand, X. Sagaert, E. Verbeken, A. Wolthuis, B. Topal, W. Everaerts, H. Bohnenberger, A. Emmert, D. Panovska, F. De Smet, F.J.T. Staal, R.J. McLaughlin, F. Impens, V. Lagani, S. Vinckier, M. Mazzone, L. Schoonjans, M. Dewerchin, G. Eelen, T.K. Karakach, H. Yang, J. Wang, L. Bolund, L. Lin, B. Thienpont, X. Li, D. Lambrechts, Y. Luo, P. Carmeliet, An integrated gene expression landscape profiling approach to identify lung tumor endothelial cell heterogeneity and angiogenic candidates, Cancer Cell 37 (2020) 421.

[23] T. Li, J. Fu, Z. Zeng, D. Cohen, J. Li, Q. Chen, B. Li, X.S. Liu, TIMER2.0 for analysis of tumor-infiltrating immune cells, Nucleic Acids Res. 48 (2020) W509–W514.

[24] M.V. Kuleshov, M.R. Jones, A.D. Rouillard, N.F. Fernandez, Q. Duan, Z. Wang, S. Koplev, S.L. Jenkins, K.M. Jagodnik, A. Lachmann, M.G. McDermott, C. D. Monteiro, G.W. Gundersen, A. Ma'ayan, Enrichr: a comprehensive gene set enrichment analysis web server 2016 update, Nucleic Acids Res. 44 (2016) W90–W97.

[25] A. Subramanian, P. Tamayo, V.K. Mootha, S. Mukherjee, B.L. Ebert, M.A. Gillette, A. Paulovich, S.L. Pomeroy, T.R. Golub, E.S. Lander, J.P. Mesirov, Gene set enrichment analysis: a knowledge-based approach for interpreting genome-wide expression profiles, Proc. Natl. Acad. Sci. U. S. A. 102 (2005) 15545–15550.

[26] M.E. Ritchie, B. Phipson, D. Wu, Y. Hu, C.W. Law, W. Shi, G.K. Smyth, Limma powers differential expression analyses for RNA-sequencing and microarray studies, Nucleic Acids Res. 43 (2015) e47.

[27] J.A. Castro-Mondragon, R. Riudavets-Puig, I. Rauluseviciute, R.B. Lemma, L. Turchi, R. Blanc-Mathieu, J. Lucas, P. Boddie, A. Khan, N. Manosalva Perez, O. Fornes, T.Y. Leung, A. Aguirre, F. Hammal, D. Schmelter, D. Baranasic, B. Ballester, A. Sandelin, B. Lenhard, K. Vandepoele, W.W. Wasserman, F. Parcy, A. Mathelier, Jaspar 2022: the 9th release of the open-access database of transcription factor binding profiles, Nucleic Acids Res. 50 (2022) D165–D173.

[28] X. Che, W. Su, X. Li, N. Liu, Q. Wang, G. Wu, Angiogenesis pathway in kidney renal clear cell carcinoma and its prognostic value for cancer risk prediction, Front. Med. 8 (2021) 731214.

[29] S. Lin, Y. Chai, X. Zheng, X. Xu, The role of HIF in angiogenesis, lymphangiogenesis, and tumor microenvironment in urological cancers, Mol. Biol. Rep. 51 (2023) 14.

[30] N.M. Kofler, C.J. Shawber, T. Kangsamaksin, H.O. Reed, J. Galatioto, J. Kitajewski, Notch signaling in developmental and tumor angiogenesis, Genes Cancer 2 (2011) 1106–1116.

[31] H.M. Verheul, E.E. Voest, R.O. Schlingemann, Are tumours angiogenesis-dependent? J. Pathol. 202 (2004) 5–13.

[32] B. Muz, P. de la Puente, F. Azab, A.K. Azab, The role of hypoxia in cancer progression, angiogenesis, metastasis, and resistance to therapy, Hypoxia 3 (2015) 83–92.

[33] N. Ferrara, K.J. Hillan, H.P. Gerber, W. Novotny, Discovery and development of bevacizumab, an anti-VEGF antibody for treating cancer, Nat. Rev. Drug Discov. 3 (2004) 391–400.

[34] Y. Zhao, A.A. Adjei, Targeting angiogenesis in cancer therapy: moving beyond vascular endothelial growth factor, Oncol. 20 (2015) 660–673.

[35] M.F. Sabbagh, J.S. Heng, C. Luo, R.G. Castanon, J.R. Nery, A. Rattner, L.A. Goff, J.R. Ecker, J. Nathans, Transcriptional and epigenomic landscapes of CNS and non-CNS vascular endothelial cells, Elife 7 (2018).

[36] Q. Zhao, A. Eichten, A. Parveen, C. Adler, Y. Huang, W. Wang, Y. Ding, A. Adler, T. Nevins, M. Ni, Y. Wei, G. Thurston, Single-cell transcriptome analyses reveal endothelial cell heterogeneity in tumors and changes following antiangiogenic treatment, Cancer Res. 78 (2018) 2370–2382.

[37] F. De Smet, I. Segura, K. De Bock, P.J. Hohensinner, P. Carmeliet, Mechanisms of vessel branching: filopodia on endothelial tip cells lead the way, Arterioscler. Thromb. Vasc. Biol. 29 (2009) 639–649.
[38] A. Bansal, S.E. Pinney, DNA methylation and its role in the pathogenesis of diabetes, Pediatr. Diabetes 18 (2017) 167–177.
[39] S.U. Kass, N. Landsberger, A.P. Wolffe, DNA methylation directs a time-dependent repression of transcription initiation, Curr. Biol. 7 (1997) 157–165.
[40] P. Beltrao, P. Bork, N.J. Krogan, V. van Noort, Evolution and functional cross-talk of protein post-translational modifications, Mol. Syst. Biol. 9 (2013) 714.
[41] L. Chen, S. Liu, Y. Tao, Regulating tumor suppressor genes: post-translational modifications, Signal Transduct. Targeted Ther. 5 (2020) 90.
[42] D. Verdegem, S. Moens, P. Stapor, P. Carmeliet, Endothelial cell metabolism: parallels and divergences with cancer cell metabolism, Cancer Metabol. 2 (2014) 19.
[43] G. Eelen, P. de Zeeuw, M. Simons, P. Carmeliet, Endothelial cell metabolism in normal and diseased vasculature, Circ. Res. 116 (2015) 1231–1244.
[44] E.M. Conway, D. Collen, P. Carmeliet, Molecular mechanisms of blood vessel growth, Cardiovasc. Res. 49 (2001) 507–521.
[45] B. Engelhardt, S. Liebner, Novel insights into the development and maintenance of the blood-brain barrier, Cell Tissue Res. 355 (2014) 687–699.
[46] D.A. Fletcher, R.D. Mullins, Cell mechanics and the cytoskeleton, Nature 463 (2010) 485–492.
[47] P.P. Provenzano, P.J. Keely, Mechanical signaling through the cytoskeleton regulates cell proliferation by coordinated focal adhesion and Rho GTPase signaling, J. Cell Sci. 124 (2011) 1195–1205.
[48] X. Guan, X. Guan, C. Dong, Z. Jiao, Rho GTPases and related signaling complexes in cell migration and invasion, Exp. Cell Res. 388 (2020) 111824.
[49] N. Byrd, L. Grabel, Hedgehog signaling in murine vasculogenesis and angiogenesis, Trends Cardiovasc. Med. 14 (2004) 308–313.
[50] G.T.K. Boopathy, W. Hong, Role of Hippo pathway-YAP/TAZ signaling in angiogenesis, Front. Cell Dev. Biol. 7 (2019) 49.
[51] R. Wu, S. Gandhi, Y. Tokumaru, M. Asaoka, M. Oshi, L. Yan, T. Ishikawa, K. Takabe, Intratumoral PDGFB gene predominantly expressed in endothelial cells is associated with angiogenesis and lymphangiogenesis, but not with metastasis in breast cancer, Breast Cancer Res. Treat. 195 (2022) 17–31.
[52] M. Teichert, L. Milde, A. Holm, L. Stanicek, N. Gengenbacher, S. Savant, T. Ruckdeschel, Z. Hasanov, K. Srivastava, J. Hu, S. Hertel, A. Bartol, K. Schlereth, H. G. Augustin, Pericyte-expressed Tie2 controls angiogenesis and vessel maturation, Nat. Commun. 8 (2017) 16106.
[53] R.J. Van Geest, I. Klaassen, I.M. Vogels, C.J. Van Noorden, R.O. Schlingemann, Differential TGF-beta signaling in retinal vascular cells: a role in diabetic retinopathy? Invest. Ophthalmol. Vis. Sci. 51 (2010) 1857–1865.
[54] L. Davis, M. Recktenwald, E. Hutt, S. Fuller, M. Briggs, A. Goel, N. Daringer, Targeting HIF-2alpha in the tumor microenvironment: redefining the role of HIF-2alpha for solid cancer therapy, Cancers (2022) 14.